The International Journal of Advanced Manufacturing Technology (2025) 138:4337–4356
https://doi.org/10.1007/s00170-025-15754-x

ORIGINAL ARTICLE

Design and development of open-source, multi-purpose wire arc additive manufacturing machine

Nithin Joseph Reddy Sagili Arthur[1] · Lei Liu[1] · João Pedro Oliveira[1]

Received: 24 January 2025 / Accepted: 10 May 2025 / Published online: 28 May 2025

Abstract
Wire arc additive manufacturing (WAAM) is a promising technology offering capabilities of high deposition rate and low processing and equipment setup cost and the possibility to create components with moderate geometrical complexity. However, wide scale industrialization of this technology is constrained by its complex thermal signature which demands an interdisciplinary approach of integrating auxiliary technologies aiming at controlling and monitoring the process often requiring costly upgrades of ancillary systems. These challenges can be addressed by developing flexible and adaptable WAAM systems that incorporate open-source solutions for developing innovative and customized auxiliary add-ons mitigating proprietary barriers and scale-up expenditures. In this work, we present the design and construction of a scalable WAAM machine featuring three-axis rectilinear motion system with a working envelope suited for small- to medium-sized components. The system integrates a customized weld torch and multiple wire feeder utilizing widely available materials to ensure functionality and cost-effectiveness. An open-source 32-bit control board is employed to achieve coordinated operation of multiple systems. A detailed assessment and selection criteria of various motion control hardware is provided. Additionally, pioneering summary of control boards with significant potential for expansion into metal additive manufacturing is also presented. To validate the machine functionality, multi-layer deposition along X–Z and multi-bead deposition along X–Y axes were conducted. These results demonstrate the seamless synchronization of the motion control, welder, and wire feeder systems, achieving defect-free depositions. Conductive and radiative electromagnetic interference mitigation measures are detailed, providing a practical guidance to simplify the development of customizable WAAM machines.

Keywords Machine design · Motion control system · Welder and wire feeder system · Electromagnetic shielding · Twin wire thin wall depositions

1 Introduction

Metal additive manufacturing (MAM) involves layer-by-layer material deposition manipulated by a digital control system, which effectively translates 3D computer-aided design (CAD) objects into machine understandable code or language to manage motion control, material deposition, and process monitoring. This process upscales productivity by reducing lead time and improves manufacturability of complex and near net shape parts. MAM has emerged as a transformative technology across aerospace, automobile, and marine industries where it significantly reduces manufacturing costs and production time. Additionally, it is gaining traction in tooling application enabling the rapid fabrication of customized dies, molds, and fixtures in various manufacturing processes [1]. To further enhance its efficiency and adaptability for large-scale industrial applications, integrating a real-time monitoring system is crucial to dynamically control process parameters [2, 3]. Research on MAM has predominantly focussed on powder bed fusion (PBF), for its ability to produce small-scale, high-quality parts with fine geometrical tolerances and on directed energy deposition (DED), for large build volume, though it often requires significant post-processing to achieve desired surface finish and dimensional accuracy [4, 5]. Processes involving powder feedstock require a closed build chamber to contain powder

✉ Nithin Joseph Reddy Sagili Arthur
n.arthur@campus.fct.unl.pt

✉ João Pedro Oliveira
jp.oliveira@fct.unl.pt

[1] CENIMAT/I3N, Department of Materials Science, NOVA School of Science and Technology, Universidade NOVA de Lisboa, 2829-516 Caparica, Portugal

particles, whereas systems using filler wire do not require such containment, making them simple and cost-effective.

The most widely used heat sources in DED are laser, electron beam, and electric arc. While laser and electron beam are high energy density sources that can produce complex design with fine tolerances, they have certain limitations. The laser energy absorption rate is lower for highly reflective metals, and an electron beam requires a vacuum environment [6]. These limitations can be significantly mitigated by employing an electric arc-based heat source, rendering the developed of wire arc additive manufacturing (WAAM). WAAM primarily utilizes four types of arc-based heat sources: (i) Gas Tungsten Arc Welding (GTAW), (ii) Plasma Arc Welding (PAW), (iii) Gas Metal Arc Welding (GMAW), and (iv) Cold Metal Transfer (CMT), which is a subtype of GMAW. In GTAW and PAW, a non-consumable tungsten electrode is used with the filler wire fed separately, whereas in GMAW and CMT, a consumable filler wire electrode is aligned coaxially with the torch. GTAW was chosen for this study due to its ability to use multiple filler wires achieving multi-material deposition and being able to have independent feed rate control, cost-effectiveness, and fine control over arc stability minimizing spatter and improving bead consistency. These benefits make GTAW ideal for developing a low cost, open-source WAAM system prioritizing affordability and material-based experimentation over high deposition rates.

Research on WAAM is broadly classified into four categories: (i) hardware systems; (ii) process and analysis; (iii) process monitoring; (iv) property characterization. Hardware systems represent the mechanical integration of arc welding machine, motion manipulator, and wire feeder system [6]. Process analysis focuses on optimizing key process parameters such as the heat input, current (I), voltage (V), wire feed rate, and torch travel speed to achieve precise and defect-free deposition. Process parameters are highly interdependent, constraining to narrow process window obtained through multi-physics simulation. Deviations from these optimal values can result in defects such as porosity, residual stresses, or surface finish ultimately affecting the quality and performance of the fabricated component [7–9]. Process monitoring involves real-time monitoring using optical, spectral, thermal, electrical, and acoustic sensor systems to detect process irregularities. With the advancements in these systems, parameters are adjusted dynamically during deposition to obtain components with better properties [10–13]. Property characterization examines the process-structure–property relationship, influencing the performance of the fabricated component [14, 15]. While exponential efforts have been focussed on most of these categories, hardware systems remain relatively underexplored as illustrated in Fig. 1. This gap is significant as the hardware systems directly impacts the scalability of WAAM technology, which is crucial for developing innovative and material based customized process solutions. Therefore, a brief review of the existing literature on WAAM machine design and development is outlined to gain insights into current work and address critical areas essential for complete WAAM machine development. Pioneering work by Anzalone et al. [16] utilized delta kinematics and a GMAW heat source, controlled by machine instruction codes for open-source WAAM. Ugla and Almusawi et al. [17, 18] further advanced open-source WAAM, integrating a welder and a cold wire feeder into a computer numerical control (CNC) machine, controlled by Arduino Mega 2560. An in-house graphical user interface was developed to generate the deposition path utilizing MATLAB replacing an open-source slicer. Cerqueira et al. [19] integrated a CMT welder with a CNC machine to study the effect of process parameters. Similarly, Lu et al. [20] adopted Anzalone's approach of delta kinematics and a GMAW welder controlled by Arduino Mega 2560. Open source Cura software was used to slice and translate the CAD file into machine instruction codes. Rosli et al. [21] improvised a Prusa i3 open-source system into a metal printer, integrating a GMAW welder using an Arduino control board. Khan et al. [22] provided a brief explanation on the construction of a gantry kinematics WAAM machine, emphasizing the importance of calibration to ensure deposition accuracy. Navarro et al. [23] developed Cartesian kinematic and wire feeder integrating GTAW welder, controlled by an Arduino Mega 2560 control board to command-and-control, and an open-source slicer to generate machine instruction codes. Their work provided a concise overview on design, development, and use of ferrite couplers for electromagnetic interference (EMI) protection. While all these studies reported the integration of motion control system with welders, none provided detailed information on hardware selection criteria, machine design and build process, multiple system integration, and most critically protection from EMI (electromagnetic interference) radiation, which hampers the customized development of WAAM.

The key challenges affecting the development of open-source WAAM are illustrated in Fig. 1. Scalability in commercial setups is hindered by the integration of evolving in situ auxiliary processes and the high costs associated with their upgrades. A cost-to-time trade-off exists, where commercial WAAM systems require high investment but offer rapid operationalization, whereas the self-build machines provide cost-effectiveness and are flexible to adapt the add-ons but necessitate interdisciplinary expertise, extensive trials, and stabilization time. Another major challenge is the limitation of open-source slicer software, where the process-dependent bead geometry requires an extensive processing through multi-physics-based simulation. Finally, the electromagnetic field disturbances cause erratic behavior in motion

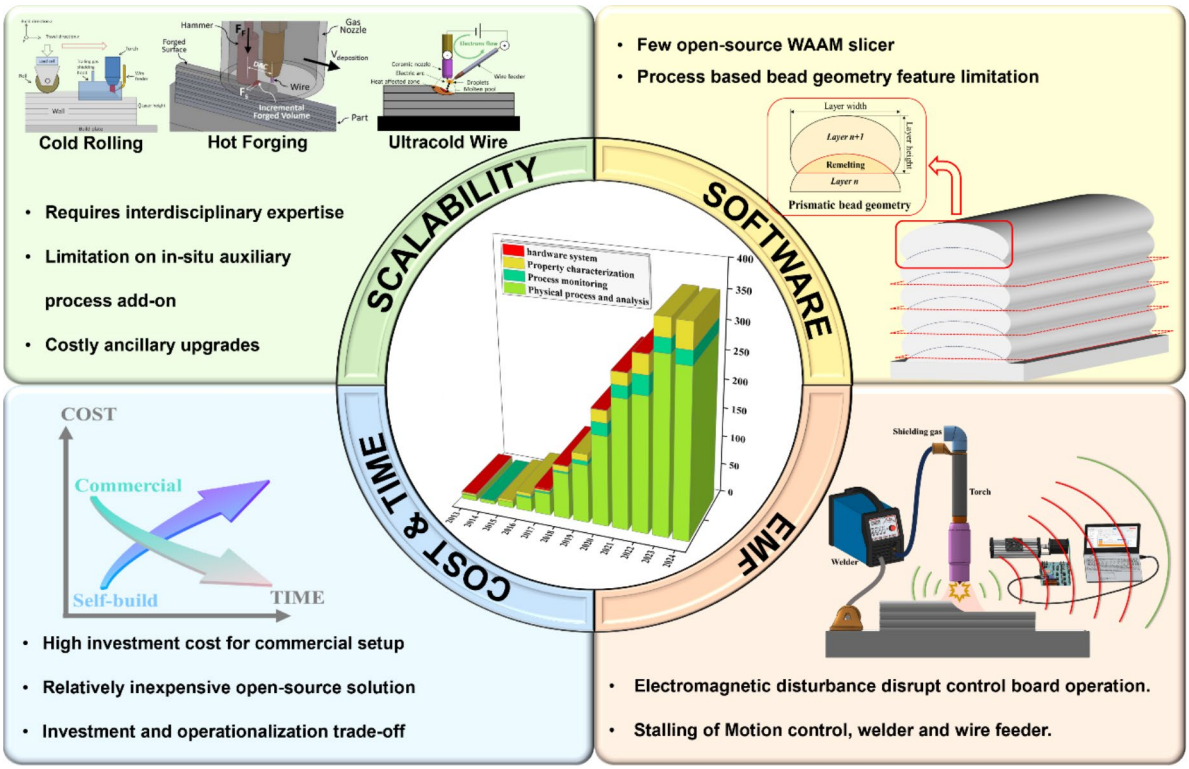

Fig. 1 Hardware system: An underexplored frontier in open-source WAAM machine development and its associated challenges

control, welder, and wire feeder systems, if not properly mitigated can significantly disrupt the process continuity.

WAAM hardware often is an integration of three core systems: (i) motion control (either robot or CNC); (ii) wire feeder system, and (iii) welder. The choice of motion control depends on a multitude of parameters, and decisive among them are the dimensions of the part, deposition accuracy, in situ processing capabilities, and cost economics. Robotic systems are well suited for large build volume and intricate geometrical features that require flexibility in orientation of the weld torch and filler wire nozzle setup. On the other hand, CNC systems provide higher accuracy and are better suited to resist vibrations induced by post-deposition process. However, the high cost of CNC systems is a significant limiting factor, with a 45% cost up for producing a titanium rib [24]. As outlined above, there is limited research on the development and implementation of open-source WAAM hardware systems highlighting the need for further research to reduce the costs associated with these setups. This work aims to address this gap by providing a comprehensive explanation focussing on the following aspects: (i) develop a structured approach for the design and development of WAAM systems, including detailed selection criteria for various open-source motion control systems such as the motor, transmission systems, and control boards; (ii) design, develop, and integrate customized weld-setup and twin wire feeder system with the motion control system ensuring a synchronized motion among them. (iii) EMI mitigation strategies implementation to create a reliable and replicable framework.

2 Materials and system integration

In this work, we envisioned to design and develop a WAAM machine that is scalable, flexible, and adaptable to support innovative applications by leveraging open-source technologies. Table 1 presents the specifications of the machine. Key features include its ability to incorporate multiple wire feeder with independent feed rate control, enabling multi-material deposition. This setup could be utilized to produce depositions either in alternating layers or together to produce functionally graded materials (FGM). The ability to deposit multi-materials using an alternating layer strategy is demonstrated in the subsequent process validation section. Constructing a WAAM machine using open-source technologies makes possible the integration of auxiliary add-ons such as cold rolling, hot forging, and ultracold wire without requiring significant hardware or software upgrades. This minimizes revenue expenditure while enhancing the machine's scalability, flexibility, and adaptability, the key performance drivers for WAAM hardware systems. The customized weld

Table 1 Specifications of WAAM machine

S. no	Specification	Details
1	Motion control	Cartesian rectilinear coordinate system with three orthogonal axis
2	Control system	Open-source 32-bit control board with RepRap firmware
3	Build volume	500 × 460 × 300 mm
4	Heat source	GTAW via 5 V relay (scalable to use diverse sources in conjunction or independently)
5	Wire feed capability	Twin wire feeder (scalable to multiple wires with control board expansion)
6	Wire feed rate	Independent feed rate control
7	Wire feeder mode of operation	Independent, alternating layer and in conjunction with variable feed rates

setup with twin wire capabilities exemplifies the adoption of scalable solutions within this framework, demonstrating how open-source technologies can support customized functionalities while maintaining cost-effectiveness.

2.1 Materials selection and construction

A critical phase in design and development process is the selection of materials and system integration, which directly influences performance, durability, and cost efficiency. The section explores the materials chosen and how different systems are assimilated to create an efficiently functioning WAAM machine. Commonly used materials include cast iron, steel (stainless and mild), aluminum, and composites in specialized applications. Aluminum extrusion profiles are extensively used in structural applications because of their superior strength-to-weight ratio, resistance to corrosion, vibration-damping properties, and modular design which supports flexible and customizable configurations [25]. In addition to aluminum, mild steel is selected for components like the bed late, substrate fixture, and weld torch which are exposed to thermal shocks and require resistance to thermal deformation [26]. While aluminum parts and stainless steel fasteners are readily available off-the-shelf, mild steel components were outsourced for manufacturing due to their large dimensions exceeding in-house fabrication capabilities. To mitigate mild steel susceptibility to corrosion, anti-corrosive coating was applied. These components make up to 102.27 kg to the total weight, for a build envelope of 500 × 460 × 300 mm (schematic shown in Fig. 3 (a)), accounting for 36% of the total hardware cost. The bill of materials used for machine construction is detailed in Sect. 3.3.

Electrical hardware, including control boards, play a critical role in ensuring precise and consistent motion during machine operation. Key components include stepper motors, 32-bit control boards, and wire harness of various gauges ranging from AWG3 to AWG24 (American wire gauge) for managing power and communication signals. Stepper motors are cost-effective and deliver high torque at lower speeds with excellent precision, making them the ideal choice for the motion control and wire feeder system. More detailed criteria for selecting the right stepper motor based on operational loads is discussed in Sect. 3.1.1. Control boards are pivotal in deciphering machine code and ensuring seamless coordination and synchronization across multiple systems. A 32-bit control board is effective in faster data processing capabilities and responsiveness, enabling real-time synchronization of multiple interconnected systems. The welder is integrated through a 5 V relay allowing precise control during the automated workflow. A more detailed discussion of the welding and wire feeder setup is provided in Sect. 3.2.

The machine frame, designed in a cube shape, requires careful attention to maintain squareness and proper alignment of the interconnected sections. The squareness of the extrusion profiles at vertices is verified using a framing square. Similarly, straightness and parallelism of the profiles and Z axis are verified by a laser marker, ensuring precise alignment over long distances. Wire harnesses were spliced, intermeshed, and twisted then soldered to create strong joint capable of spanning long distances. These wires were crimped with female crimp pins inserted into connector housing and plugged into the control board header pins. Finally, wire harnesses were routed through cable chain to prevent tangling while providing the necessary mobility for the interconnected axes.

2.2 Open-source software

Parametric modelling software is extensively utilized for designing machine components, performing interference checks within the kinematic envelope and extracting bill of materials from the final design. Open-source software such as FreeCAD, SolveSpace, OpenSCAD, and free-for-use software like Onshape and Fusion 360 offer robust features for designing components, structural frame, and complex assemblies. CAD modelling for deposition is exported in standard tessellation language format and processed through custom-built python script for generating required machine code. Python script for thin-wall depositions is provided as a Supplementary Information. This approach is tailored for the development of a custom-built WAAM machine that

requires assimilation of motion control, wire feeders, and an external welder.

Motion control is simulated in a CNC viewer software to visualize the deposition path ensuring repeatability of the layer-by-layer deposition process. RepRap firmware adapting to National Institute of Standard and Technology (NIST) G-Code interpreter is employed to control the canonical machine's function and is highly suitable for machines requiring customized configurations [27]. A comprehensive explanation of various open-source firmware and supporting kinematics is provided in Sect. 3.1.3.

3 Design and assembly

In the construction of this machine, attention was placed on cost-effectiveness, functionality, and simplicity of design—a core tenet of Design for Manufacturability and Assembly (DFMA) [28, 29]. The design emphasized a modular setup adaptable to various processes, with a focus on ergonomics to minimize human fatigue. While many commercial systems rely on proprietary technologies and closed architectures, our approach leverages open-source components and a modular design to adapt for evolving innovative and customized solutions. This translates to significant long-term cost savings and greater adaptability to cater research and industrial needs. Furthermore, this machine incorporates twin wire feeder for multi-material deposition, expanding material capabilities which is on par with entry-level commercial systems. This section provides a detailed explanation of the operational and functional criteria of the system and components used while maintaining a cost-effective and adaptable framework.

3.1 Motion control

The developed WAAM machine employs a Cartesian coordinate-rectilinear kinematic that allows for precise motion along three orthogonal axes. This setup is relatively simple to build and configure eventually narrowing down time and cost. Motion control comprises of an actuator (made up of a stepper motor and a transmission system) and control board to provide the necessary linear motion. This section is further divided into motor, transmission, and control board providing insights on each of them.

3.1.1 Motor

Stepper motors are ideal for executing complex motion tasks with high precision and accuracy. Rotor movement in discrete steps, better known as stepping, and ease of integration with control boards make them the best choice for motion control and feedstock extrusion in MAM. These motors provide adequate torque at lower speeds, as the torch movement in WAAM is generally slower compared to conventional machining operations. Two criteria that decide the selection of the stepper motor are compatibility with the control board and operational load. The winding arrangement (either unipolar or bipolar) and rated current influence the compatibility of the stepper motor with the control board while the torque required to move the gantry system dictates the operational load characteristics. A detailed explanation of torque calculation using empirical relation is provided below.

Torque $\left(T_M\right)$ is the force required to rotate an object about its axis and is divided into two components: load torque and acceleration torque; empirical relation is provided in Eq. 1. Load torque $\left(T_L\right)$ refers to the torque necessary to move the gantry and overcome the friction of the interconnected components, while acceleration torque $\left(T_a\right)$ is the additional torque required during acceleration and deceleration phases of the gantry's motion; empirical relations are provided in Eq. 2 and Eq. 3 respectively. Key variables involved in calculations include the following: force (F) in the moving direction in N, lead screw lead $\left(P_B\right)$ in mm, η is the efficiency of lead screw around 60 ~ 70%, J_0 is the rotor inertia in kg-m^2, J_L the load inertia in kg-m^2 and N_m is the axis speed in RPM, t_1 is the acceleration and deceleration time in seconds, s. A safety factor between 1.5 ~ 2 is typically applied to account for any variations or uncertainties [30].

$$Total\ torque, T_M = \left(T_L + T_a\right) \times S_f \tag{1}$$

$$Load\ torque, T_L = \left(\frac{FP_B}{2\pi\eta}\right) \tag{2}$$

$$Acceleration\ torque, T_a = \frac{\left(J_0 + J_L\right)}{9 \cdot 55} * \frac{N_m}{t_1} \tag{3}$$

Stepper motors are directly coupled to the lead screw and positioned on top of it, driving the supervening axis of the gantry system. This configuration helps mitigate the effects of radial and axial loads that the motor needs to counter. Selecting a suitable motor involves confirming several criteria after completing the torque calculations. The motor winding type, whether unipolar or bipolar, must be compatible with the control boards; for example, a unipolar motor with five or six leads cannot interface with a control board designed for bipolar motor. Additionally, rated current must be carefully chosen to prevent overheating and potential damage from excessive current flow through windings. A suitable step angle (either 0.9° or 1.8°) that determines the number of steps per revolution must be chosen based on the required positional accuracy while considering the effects of inductance and back electromotive force (EMF),

which occurs during changes in current direction. Finally, the motor adhering to the mounting flange dimensions or frame size specified by National Electrical Manufacturers Association (NEMA) standards, ensuring compatibility with the system design and torque requirements, is chosen [31]. NEMA 23 high torque (24.5 kg.cm) stepper motor with a step angle of 1.8° per step and with an accuracy of ±5% is used for all the axes ensuring precise and reliable motion control [32].

3.1.2 Transmission

A transmission system translates rotary motion into linear motion along an axis with a minimum torque loss from the stepper motor. A brief overview of commonly deployed transmission systems in CNC and 3D printers includes timing pulley and belt, ball screw drive, lead screw drive, and rack and pinion. Schematics of the various transmission systems are shown in Fig. 2. Timing pulley and belt drives are well suited for applications with low load inertia but are prone to racking issues and require the belt to be held in constant tension. Ball screw drives and lead screws are similar in operation, and key difference among them is the mounting nut preloaded with steel balls to minimize friction and improve the efficiency in the ball screw drive. Both drives experience whipping due to the screw shaft flexing over long travel lengths; however, this is alleviated by ensuring proper tensioning at the mounting ends. Rack and pinion systems are best suited for heavy duty applications due to their robust and simple construction. Similar to the rack and pinion option, lead screw drives are also prone to backlash issues; however, the use of anti-backlash nuts can mitigate this issue [33].

To finalize the selection of the transmission system, it becomes imperative to account for calibration requirements. As the Y and Z axes are driven by multiple actuators as shown in Fig. 3 (a), tilt and twist misalignments along these axes are corrected using least-squares algorithm to minimize the sum of height errors. This demands a transmission system that can accommodate these corrections, which necessitates to avoid rigid structures with very fine tolerances. Additionally, heavier transmission systems would increase the weight of the gantry mandating heavy-duty stepper motors. Two variants of lead screw drives were employed: (i) lead screw with guide rod for Z axis and (ii) C-beam lead screw bundle for X and Y axes shown in Fig. 3 (c) and (e) respectively. An overview of

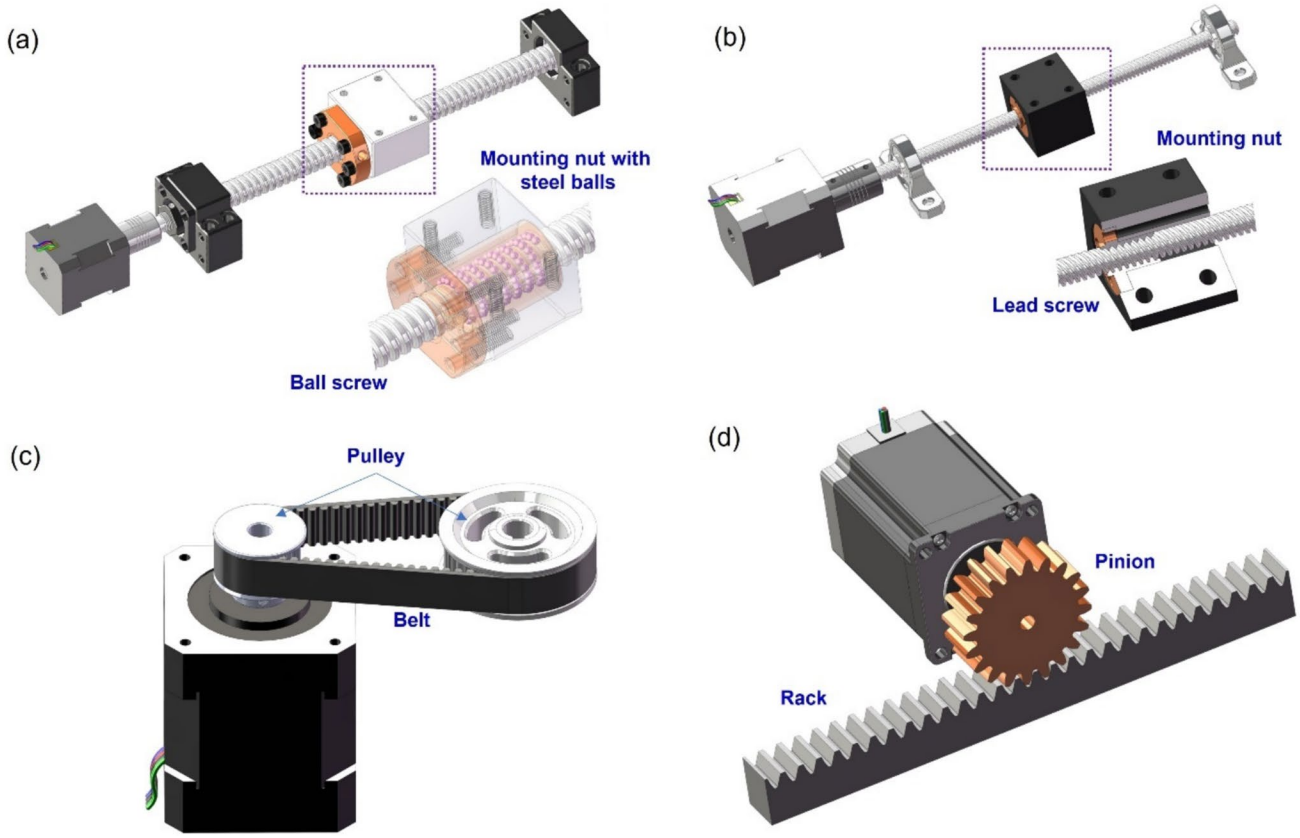

Fig. 2 Transmission systems: (**a**) ball screw drive, (**b**) lead screw drive, (**c**) timing pulley and belt, (**d**) rack and pinion

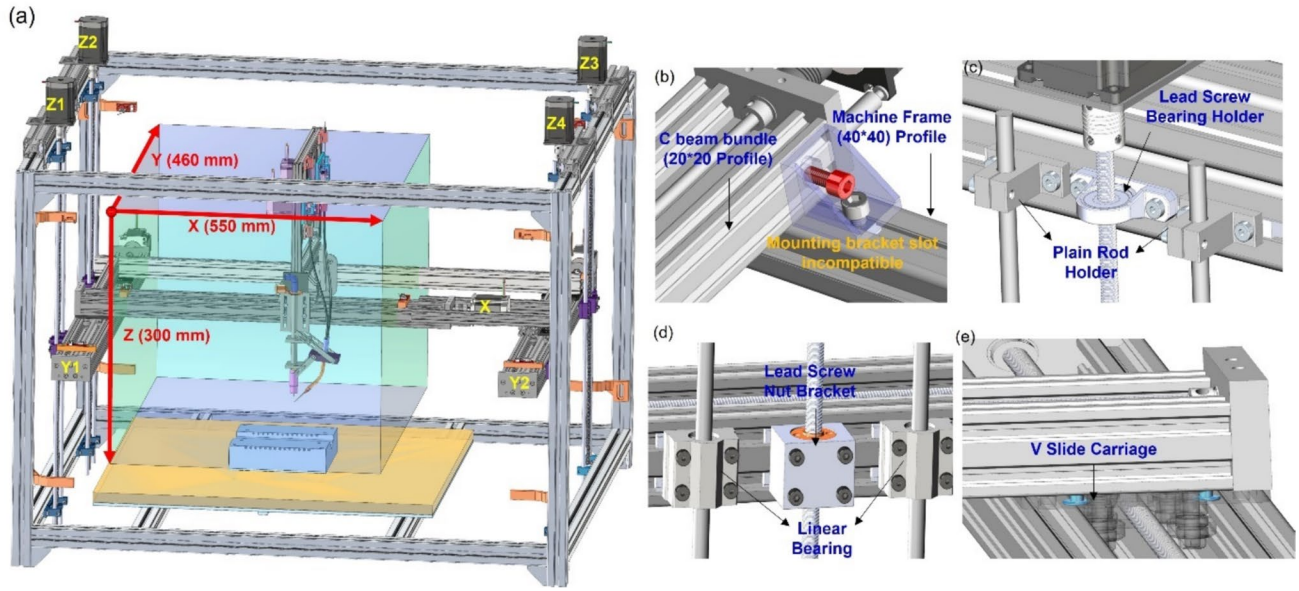

Fig. 3 (**a**) Machine schematic with working envelope, (**b**) C beam bundle interference with machine frame, (**c**) lead screw with guide rod mounting to machine frame, (**d**) lead screw with guide rod mounting to C beam bundle, (**e**) C beam lead screw bundle

these two systems and empirical relations for selecting appropriate lead screw sizes is explained hereafter.

The 8 mm TR 8*8, trapezoidal lead screw was directly coupled to the stepper motor through a coupler, with guide rods placed parallelly in the guide rod setup for Z axis, while two pairs of rollers slide along the extrusion profile in the C-beam bundle for X and Y axes, providing the necessary load bearing support. The trapezoidal lead screw traverses through an anti-backlash nut enhancing repeatability and smooth bidirectional linear motion with an accuracy of 0.05 to 0.10 mm [34]. A lead screw with guide rod setup was chosen for the Z axis, as the 20 series extrusion of C-beam bundle is incompatible with 40 series extrusion of the machine frame as illustrated in Fig. 3 (b). To select the appropriate lead screw size, the superposition method is used to calculate the deflection between two hinged supports [35]. Empirical relations of various load configurations are given in Fig. 4. Variables in the empirical relations are as follows: P is the point load in N and w is the uniform varying load in N/m, E is the modulus of elasticity in Pa, I is the area moment of inertia in m^4, b is the sub-length in m.

3.1.3 Control board

A control board is a printed circuit board (PCB) integrating a processor and peripherals to coordinate stepper motors, sensors, and ancillary systems according to user-defined programs. PCBs are categorized based on their data processing capabilities, which are determined by two key factors data width and processing frequency. Data width refers to the amount of data that can be processed within a given timeframe, while processing frequency indicates the speed at which the control board can execute commands. Both are vital for seamless integration of multiple systems. A simple flowchart to aid the selection of appropriate control board is shown in Fig. 5. A comprehensive list of 32-bit boards used in additive manufacturing processes, with five or more stepper motor operability is benchmarked in Table 2. A WAAM machine with an integrated wire feeder system requires five or more stepper motors, four for motion control (X, Y, and dual Z axes), and one for wire feeding.

Onboard hardware scalability reduces the complexity of electrical architecture and configurations. Table 3 highlights various opensource firmware and supporting kinematics for the control boards listed in Table 2, with most of them are written in C and C++languages. The firmware deciphers the machine instruction codes into electrical signals that direct the hardware to perform the intended actions. The selected kinematic firmware configuration is then flashed onto control board, setting kinematic envelope, process functionalities, and to execute print files.

A control board schematic is shown in Fig. 6. A 24 V power supply unit (PSU) powers the control boards in accordance with the recommended specifications. Two control boards, a main board, and an expansion board are used to operate the nine stepper motors for the motion control and feedstock extrusion control system The boards communicate through CAN (Controller Area Network) protocol using RJ11 cables (Registered Jack 11), with each assigned unique address to enable scalability for future hardware additions. The Z axis is driven by four independent motors that are connected to the main board, while the X and Y axis are

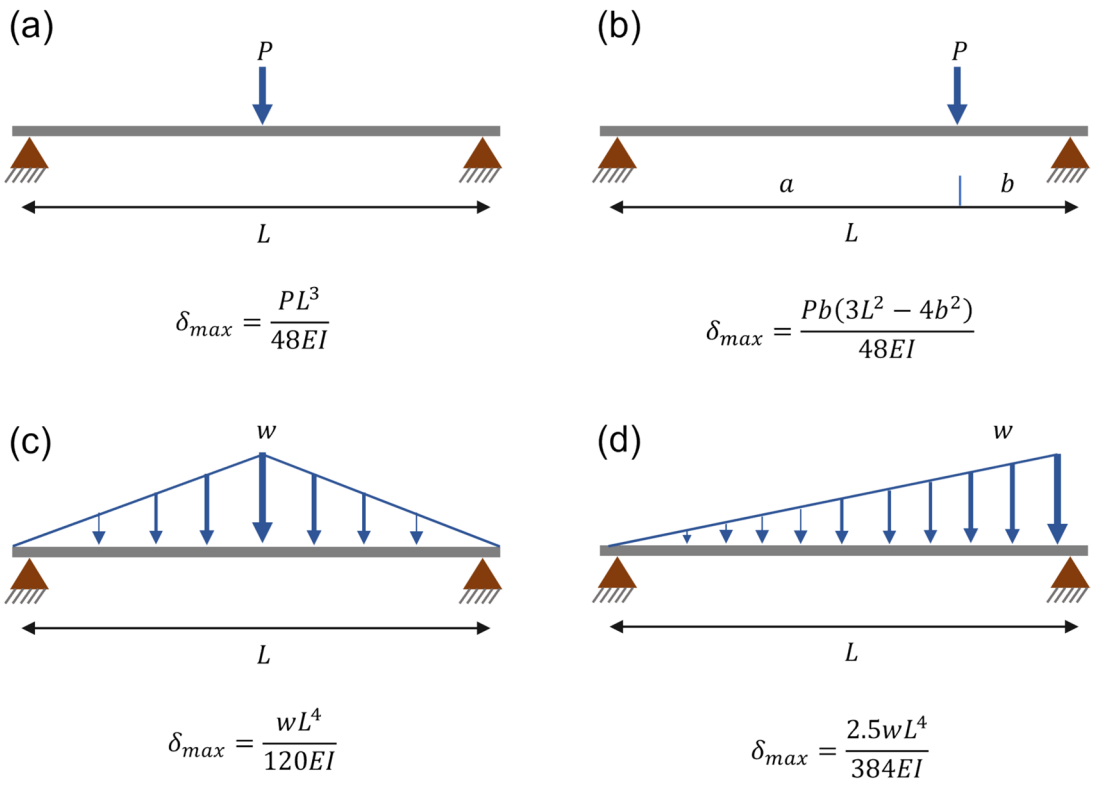

Fig. 4 Method of superposition, maximum deflection: (**a**) midspan point load, (**b**) load at any point, (**c**) triangular load distribution, (**d**) uniformly varying load

connected to the expansion board as shown in Fig. 6. This arrangement was done to match the order of endstop to the stepper motor to perform ¨Axis Levelling using End Stop¨, enabling axis calibration to correct for any major positional deviations. This setup corrects actuator misalignments, preventing parallelism errors between the gantry and bed plate that could compromise bead geometry. To limit axis overtravel during any manual operation, an endstop is installed at the maximum envelope position for each axis, as depicted (indicated by endstop mounting bracket at the terminal position of the line arrow) in Fig. 3 (a). A two-position emergency push button (normally closed and normally open) is installed to immediately halt machine operation when triggered [49]. Two brushless DC motor fans are installed inside the junction box to prevent the control boards from overheating. A human machine interface (HMI) was established between the control board and laptop through a RJ45 connection.

3.2 Weld set-up and twin wire feeder

Direct current electrode negative (DCEN) mode is chosen to achieve high deposition rates with better dimensional accuracy, with the negative electrode fixed to the weld torch and the positive electrode to the substrate fixture completing the welding circuit [50, 51]. To insulate the interconnected systems from potential electromagnetic interference (EMI) caused by the welding circuit, a cost-effective insulator, such as a wooden plank, is placed between the bed plate and the machine frame.

The welder is interfaced with the control board by configuring a two-state normal relay as a welder controller to toggle on and off sequence. Digitally, macro files for both torch on and torch off are sequenced in the print file to control the welder operation.

Stepper motors are chosen for the wire feeder system over conventional DC motors, as they provide precise control over the wire feed rate. The wire feeder system consists of two rollers, a grooved driver roller attached to the stepper motor shaft and a plain driven roller housed in a mounting bracket. As the roller rotates, the filler wire is drawn from the wire spool positioned at the top of the machine frame into the roller junction through a flexible steel hose to prevent wire entanglement. Coordinated and synchronized operation of the weld torch and wire feeder is essential for WAAM. This could be achieved by configuring the wire feeder either as an additional motion system or as an extruder, each with its own operation characteristics and limitations as explained hereafter.

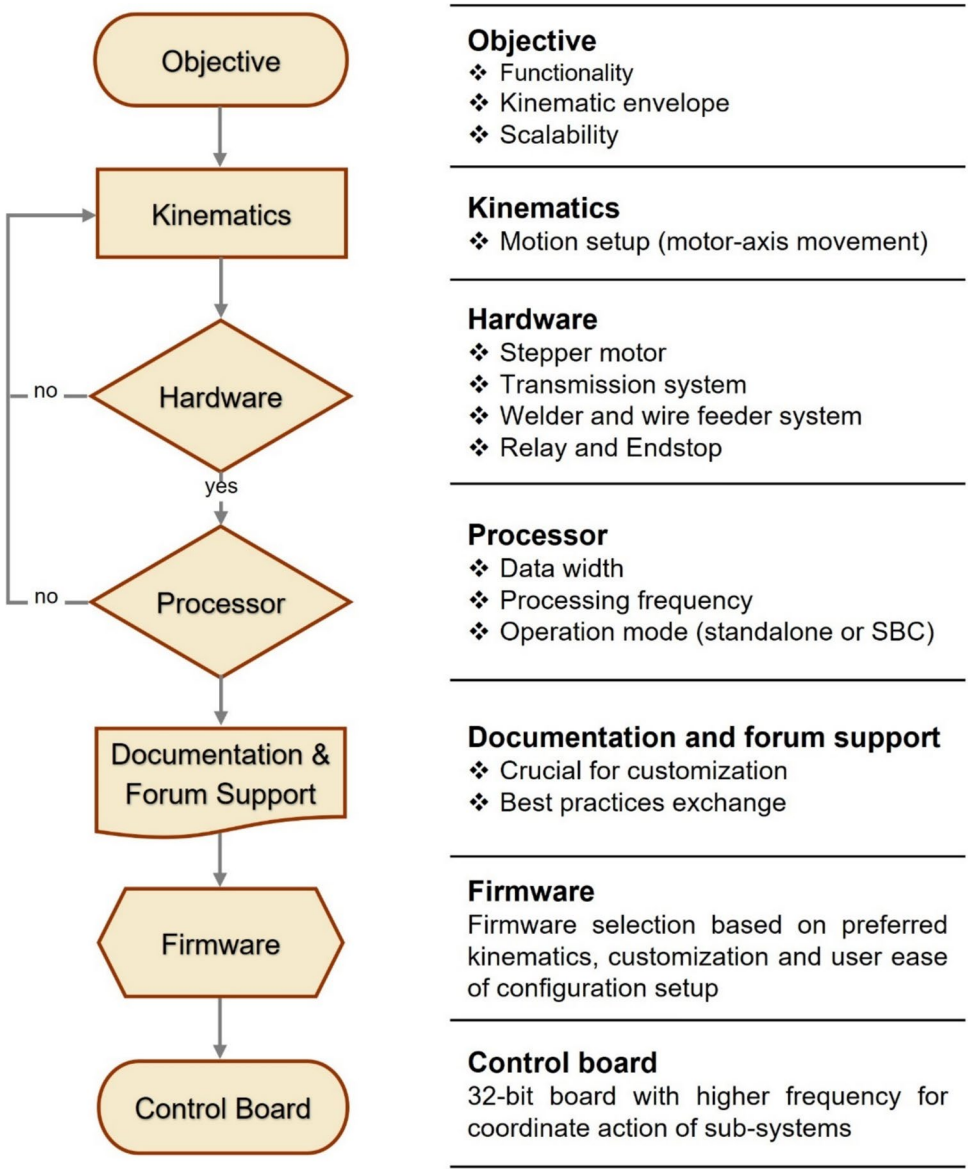

Fig. 5 Control board selection flow chart

In the first option, wire feeders are configured as secondary motion control system which allows for independent wire feed rate relative to the weld torch travel rate which is controlled by the primary motion control system. In this configuration, while torch travel speed and wire feed rate are coordinated, they operate asynchronously, with a constant wire feed rate maintained throughout deposition. For the second option, wire feeders are configured as extruders in the primary motion control system. The torch travel speed and wire feed rate can be varied for each deposition layer controlled by an "F" parameter (feed rate per minute), resulting in coordinated and synchronous feed rates. The circuit diagram for the welder and wire feeder system is shown in Fig. 7 and a schematic view is depicted in Fig. 8 (b). The choice between these configurations depends on the materials being deposited, process parameters, and the desired deposition strategy.

3.3 Machine design

This section outlines the critical aspects of machine design that significantly impact on functionality and cost-effectiveness. One of the key considerations is the control mode of stepper motors. Closed-loop stepper motors, also referred to as stepper servos, comprise an encoder and a PID controller (proportional-integral-derivative) to monitor and control discrepancies between target and actual position. The controller receives input signals representing the intended and current positions, calculates the error, and adjusts the motor's movements using proportional,

Table 2 List of 32-bit control boards used for additive manufacturing

No	Company	Board name	Processor			Firmware
			Family	Data (bit)	Frequency (MHz)	
1	Duet [36]	Duet 3 Mainboard 6HC	ARM Cortex M7	32	300	RepRap
2		Duet 3 Mainboard 6XD	ARM Cortex M7	32	300	RepRap
3		Duet 3 Mini 5 +	ARM Cortex M4 F	32	120	RepRap
4		Duet 2	ARM Cortex M4 F	32	120	RepRap
5	Big Tree Tech [37]	Manta M5P	ARM Cortex M0 +	32	64	Klipper
6		Manta M8P V1.1	ARM Cortex M0 +	32	64	Klipper
7		Manta M8P V2.0	ARM Cortex M0 +	32	550	Klipper
8		SKR 3	ARM Cortex M7	32	480	Marlin, Klipper, RepRap
9			ARM Cortex M7	32	550	Marlin, Klipper, RepRap
10		SKR3 EZ	ARM Cortex M7	32	480	Marlin, Klipper, RepRap
11			ARM Cortex M7	32	550	Marlin, Klipper, RepRap
12		SKR V1.4	ARM Cortex M3	32	100	Klipper
13		SKR V1.4 Turbo	ARM Cortex M3	32	120	Klipper
14		SKR Pro V1.2	ARM Cortex M4	32	168	Marlin
15		Octopus Pro V1.0/V1.1	ARM Cortex M7	32	550	Marlin, Klipper, RepRap
16			ARM Cortex M4	32	180	Marlin, Klipper, RepRap
17			ARM Cortex M4	32	168	Marlin, Klipper, RepRap
18		Octopus Max EZ	ARM Cortex M7	32	550	Marlin, Klipper
19		Kraken	ARM Cortex M7	32	550	Marlin, Klipper, RepRap
20	Lerdge [38]	Lerdge-Z	ARM Cortex M4	32	168	Marlin, Klipper
21	Smoothieboard [39]	Smoothieboard 5X	ARM Cortex M3	32	120	Smoothieware
22	Archim2	Archim2	ARM Cortex M3	32	84	Marlin
23	Panucatt [40]	Azteeg X5GT	ARM Cortex M3	32	120	Smoothieware
24	Aus3D [41]	Rumba 32	(No Info.)	32	180	Marlin
25	Max3 dshop [42]	RADDS	ARM Cortex M3	32	84	Repeiter, Marlin
26	Thing-Printer [43]	Replicape + BeagleBone Black	ARM Cortex A8	32	200 (PRU) + 1000 (CPU)	Redeem
27	(Self-build)	RemRam	ARM Cortex M7	32	216	Marlin
28	(Self-build)	Generation 7	ARM Cortex M0 +	32	48	RepRap

Table 3 Firmware and supported kinematics

S. no	Company	Supporting kinematics
1	Marlin [44]	Cartesian, Core (H-Bot), Delta, and SCARA
2	Klipper [45]	Cartesian, CoreXY, Delta
3	RepRap [46]	Cartesian, Core XY, Core XZ, Core XYU, Core XYUV, Linear Delta, Rotary Delta, IDEX, Markforged, Serial SCARA, Five-bar parallel SCARA, Hangprinter, Polar
4	Smoothieware	Cartesian, Delta, Hbot, Core-XY, Rotary Delta, Morgan Scara
5	Repeiter [47]	Cartesian, Core XYZ, Delta, Dual X axis
6	Redeem [48]	Cartesian, H-Belt, Core XY, Delta

integral, and derivative actions to ensure precise control. Most control boards do not have in-built hardware capabilities to support closed-loop control which necessitates additional control boards. Additionally, closed-loop stepper motors are equipped with electromagnetic brakes to hold position during emergency stop or power loss. Implementing a closed-loop setup increases the cost by eight times compared to open-loop system and up to ten times if electromagnetic brakes are included. In the construction of this WAAM machine, open-loop stepper motors are used as they provide the desired functionality. Alternative to electromagnetic brakes, mechanical

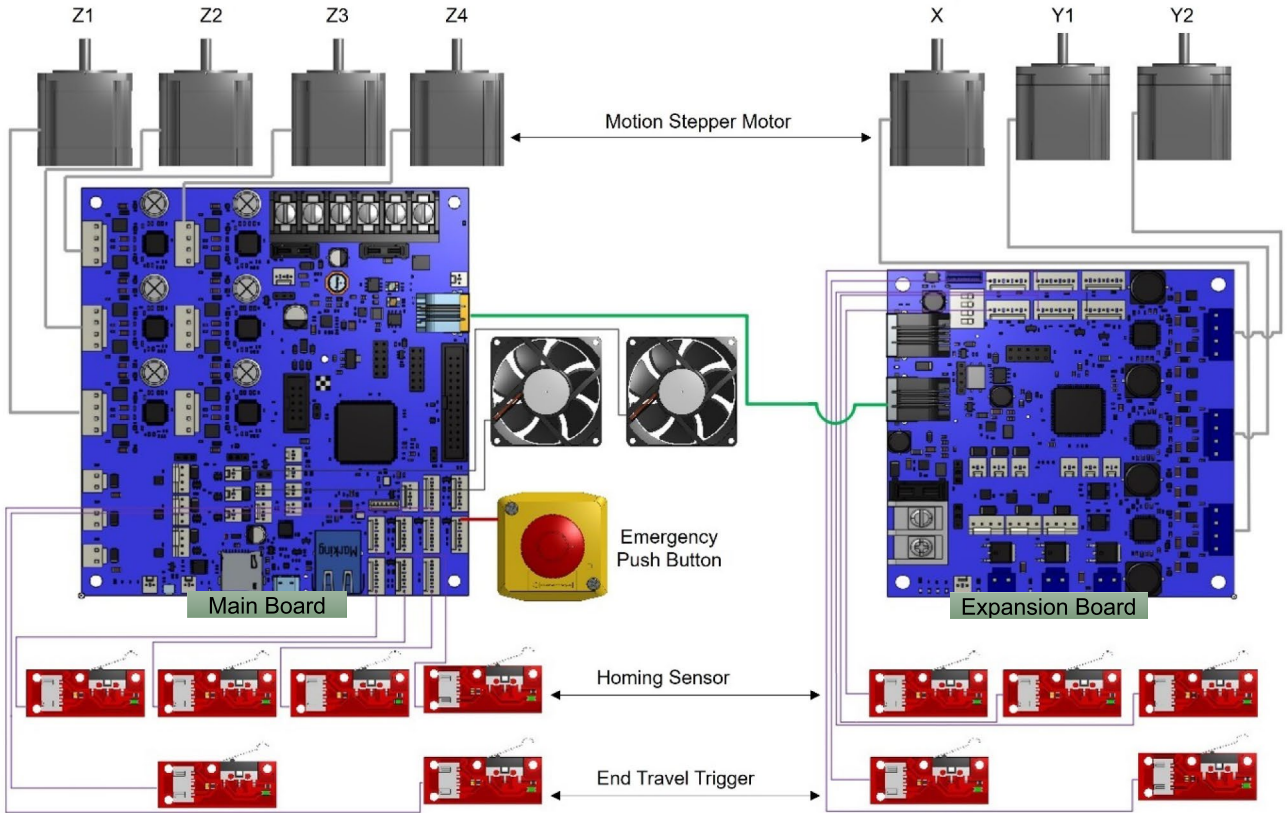

Fig. 6 Motion control system circuit diagram

stoppers are installed to prevent the accidental collision of the gantry with the bed plate as marked in Fig. 8 (a).

The machine frame is constructed using 40 series aluminum extrusion profiles, due to their higher load bearing capacity and resistance to deflection, which are vital for maintaining structural integrity. Additionally, these profiles provide superior vibration damping compared to smaller profiles such as the 20 or 30 series extrusion profiles, making them the ideal choice for structural applications. A total of 16.2 m of these extrusion profiles were used, contributing 28.8 kg to the total weight. With a section modulus of 5281.65 mm^3, the 40*40 extrusions provide the necessary structural support to withstand a total load of 185 kg (assuming a safety factor of 2.0). This includes the static load of 55 kg inclusive of bed plate, substrate fixture and substrate plate, 36 kg for the gantry system, and a component (part deposition) weight of 94 kg. Optimal selection of profiles aids in reducing the cost and weight of the structure, as they represent a significant portion of the construction materials.

Electromagnetic interference (EMI) is the impairment of an electromagnetic signal by an electromagnetic disturbance as defined by IEEE standards [52]. In welding operations, high-frequency noise is generated at the onset of the electric arc between the electrodes. These disturbances can take place either as radiated or conducted signals that induce unwanted signals in the motion control circuits leading to erratic motor behavior and relay malfunctions. Initial trials revealed frequent disconnections in the motion control circuit and cases where the welder relay did not switch off as intended at the end of the deposition path. To mitigate these effects and to ensure electromagnetic compatibility (EMC) of the system, the following measures were implemented. Shielded cables, featuring conductive foil wrapped around the core, were employed for stepper motors and sensors to block external noise. Additionally, a Faraday cage was setup around the working boundary to conceal the radiated EMI waves, preventing it from affecting the motion control system (refer to Fig. 8 (b)). Ferrite chokes were utilized to suppress high-frequency noise by creating inductive impedance, dissipating the interference as heat. It is also crucial to avoid high frequency welders as they generate high voltage at the start to initiate and maintain arc stability exacerbating EMI issues. Finally, the machine frame was grounded as it provides a path to safely dissipate unwanted electrical noise. These measures minimized disruptions from EMI and improved the reliability of the systems throughout the process [53].

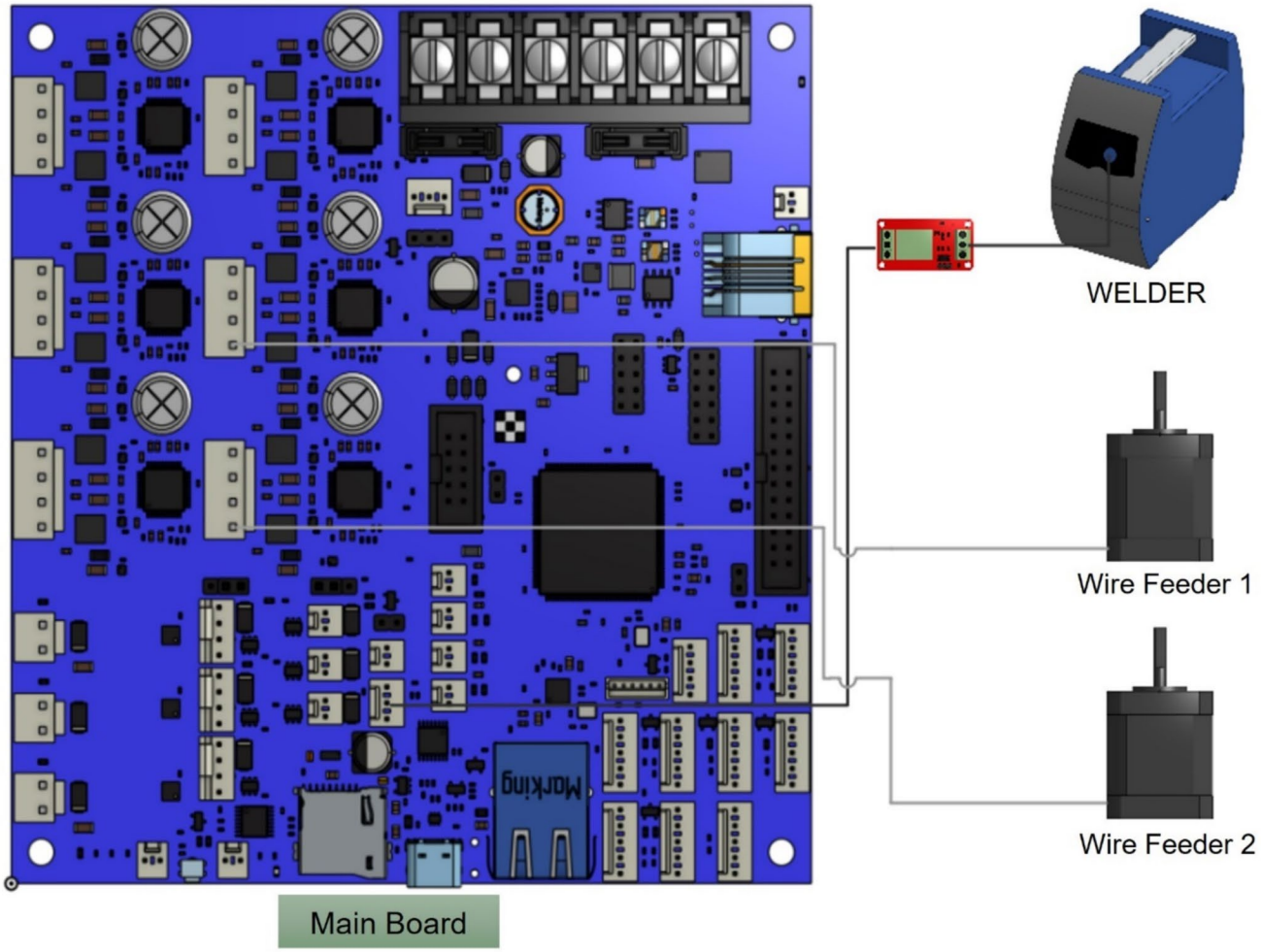

Fig. 7 Welder and wire feeder circuit diagram

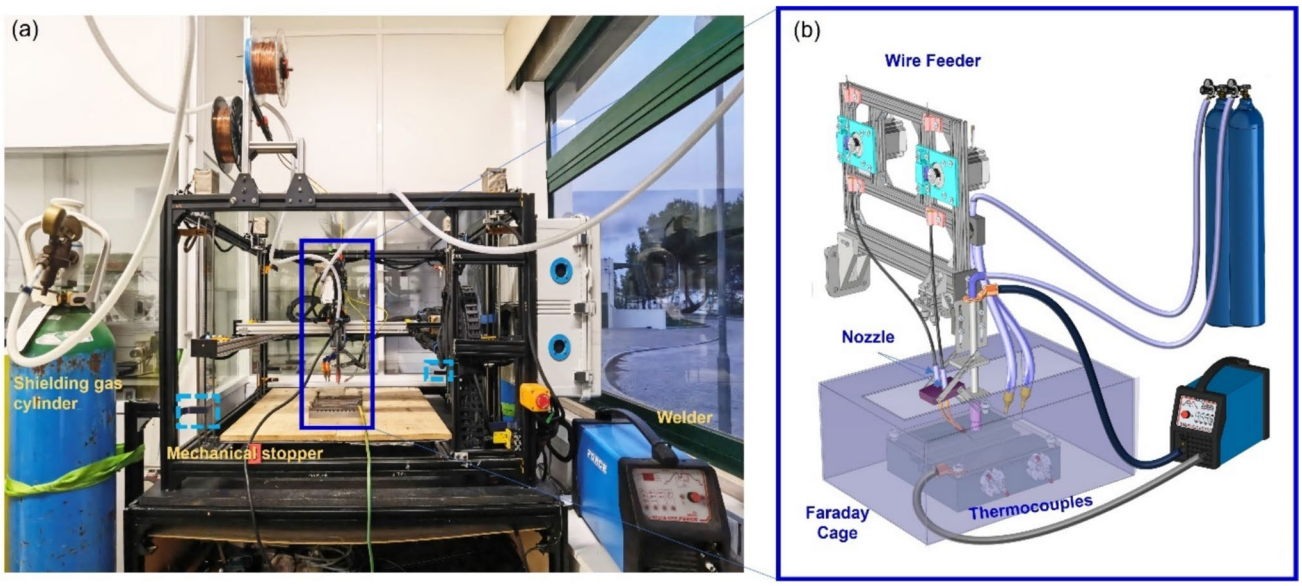

Fig. 8 (**a**) Self-developed WAAM machine, (**b**) schematic of welder and wire feeder system with shielding gas setup

Table 4 Bill of materials

No	Specification	Component	Quantity	Total weight (kg)	Total cost (euros)
Machine frame					
1	Aluminum	40*40 extrusion profiles	16.2 m	28.83	388.80
2	Aluminum	40 series connectors	44 units	1.14	46.54
3	Aluminum	20*40 extrusion profile	0.78 m	0.66	9.79
4	Aluminum	20 series connectors	6 units	0.04	4.28
5	Stainless steel	Fasteners	1 set	1.90	62.18
Z-axis					
6	NEMA 23	Bipolar stepper motor	4 units	5.20	135.10
7	Aluminum	Mounting plate	4 units	0.12	24.99
8	Stainless steel	Plain rod	8 units	4.00	77.64
9	Stainless steel	Lead screw – TR8*8	4 units	1.60	97.02
10	Aluminum	Support bearings	24 units	0.64	47.92
11	Aluminum	Linear bearings	8 units	0.40	27.16
12	Aluminum	Connecting block	4 units	0.30	26.57
13	Brass	Anti-backlash nut	8 units	0.09	19.19
14	Aluminum	Flexible coupler	4 units	0.06	9.20
15	Aluminum	20*40 extrusion profile	1.07 m	0.91	13.49
16	Sensor	Endstop	6 unit	0.02	18.45
17	Polymer	Cable chain	1 set	0.70	55.79
18	Stainless steel	Fasteners	1 set	1.10	80.21
X and Y axes					
19	Aluminum	C Beam linear bundle	3 set	8.41	379.81
20	NEMA 23	Bipolar stepper motor	3 units	3.9	101.33
21	Aluminum	20*40 extrusion profile	4.52 m	3.73	57.12
22	Aluminum	20 series connectors	34 units	0.21	24.25
23	Sensor	Endstop	5 units	0.02	15.38
24	Polymer	Cable chain	2 set	0.88	63.17
25	Stainless steel	Fasteners	1 set	0.36	35.33
Bed plate and substrate fixture					
26	Mild steel	Bed plate	1 unit	36.38	534.00
27	Wood	Wooden plank	1 unit	2.50	7.99
28	Mild steel	Substrate fixture	1 unit	13.59	179.00
29	Mild steel	Substrate plate	1 unit	2.15	67.50
30	Stainless steel	Fasteners	1 set	0.31	16.31
Weld setup and wire feeder					
31	TIG	Welder	1 unit	9.5	1,428.00
32	Mild steel	Torch housing	1 unit	0.14	105.00

Table 4 (continued)

No	Specification	Component	Quantity	Total weight (kg)	Total cost (euros)
33	Copper	Collet & collet holder	1 unit	0.02	4.22
34	Tungsten	Electrode	1 unit	0.01	11.94
35	Stainless steel	Fasteners	1 set	0.01	1.33
36	NEMA 23	Bipolar stepper motor	2 unit	2.6	67.55
37	ABS	Motor mounting bracket	2 unit	0.10	-
38	Aluminum	20*40 extrusion profile	1.38 m	0.82	13.91
39	Aluminum	20 series connectors	10 units	0.06	7.13
40	Stainless steel	Fasteners	1 set	0.21	10.50
Control board and wire harness					
41	ABS	Junction box	1 unit	4.76	119.13
42	24 V	Power supply unit (PSU)	1 unit	0.76	44.50
43	32 bit	Control board – main	1 unit	0.22	276.57
44	32 bit	Control board – expansion	1 unit	0.20	115.00
45	2 position (NC + NO)	Emergency push button	1 unit	0.06	7.87
46	5 V, 2 position	Relay	1 unit	0.01	3.69
47	AWG 3,13,22,24	Wire harness	1 set	1.52	269.68
48	AWG 3,13,22,24	Connector and terminal	1 set	0.08	3.41
49	PET braided	Cable protection sleeve	1 set	0.20	289.67
Shielding gas – pneumatic accessories					
50	20 l/min flow rate	Shielding gas flow meter	1 unit	1.95	158.00
51	Polymer	Shielding gas hose	1 set	0.79	15.67
52	Stainless steel	Hose clip	1 set	0.10	9.34
Hardware cost				**144.5**	**5,588**
No	Role			Cost per man-day	Total cost
Manpower cost					
53	Supervisor			115	17,250
54	Engineer			40	12,000
Manpower cost					**29,250**
Total machine cost (including hardware and manpower)					**34,838**

Table 4 provides comprehensive bill of materials classified into various subassemblies aiding in planning and cost estimation. Notably, tools and consumables are excluded as they do not represent capital investment. Manpower costs which constitute to 84% of the total machine cost reflect the extensive efforts involved from planning and design stages to stabilization. A considerable portion of these costs stemmed from intensive work needed to finalize hardware specifications and address issues related to EMI. The overall cost of machine including hardware and manpower amounts to 34,838 euros, reflecting cost standards prevalent in Portugal, where both the per-day manpower cost and product procurement were set. This cost is significantly lower compared to commercial machines

highlighting the cost savings and flexibility that can be achieved through a self-built approach.

4 Process validation

4.1 Multi-layer deposition

Thin wall depositions were performed to validate machine performance, using stainless steel alloy (Er 316L Si) for single wire setups and a combination of stainless steel alloy (Er 316L Si) with nickel-based alloy (Er NiCrMo-13) for twin wire feeder setups, both with a wire diameter of 1.2 mm, as shown in Fig. 9. Both depositions involved 20 layers along a unidirectional path, with material deposition along the X axis and layers built sequentially along the Z axis. These depositions are ideal for assessing motion control repeatability over geometries that require extensive tool path optimization. The weld setup and twin wire feeder system were validated using an alternate layer strategy, where stainless steel and the nickel-based alloy were deposited in successive layers to evaluate wire feeder system's ability to switch-over seamlessly while remaining synchronized with the welder and motion control systems. Cross-sectional microstructural analysis confirms defect-free depositions.

Multiple trials of single bead depositions were performed to determine optimal process variables, which were subsequently applied to overlapping beads. The deposition efficiency calculated using total wall width (TWW) and effective wall width (EWW) was 77.2% for single wire deposition, significantly higher than efficiencies achieved in comparable nickel based GTAW depositions [54, 55], [56–62], as shown in Fig. 9 (c). Typical columnar dendrites could be observed at the bottom and middle regions as shown in Fig. 9 (d) and (e). While an equiaxed dendritic structure is observed in the top region as shown in Fig. 9 (f). This variation in microstructure morphology is due to the evolving thermal gradients and solidification rates along the deposition direction, corresponding to maximum heat extraction. Distinct layer boundary is marked by dashed lines in Fig. 9 (d), due to partial remelting of the previous layer. Similar microstructures were also reported for other nickel-based alloys [63, 64].

Figure 10 depicts the twin wire deposition, contrary to single wire deposition a significant bead collapse is observed due to the same process parameters being applied to different materials (Er 316L Si and Er NiCrMo-13) with distinct thermophysical properties. Layers corresponding to the respective materials are identified by their saturation hue as shown in Fig. 10 (c)(d)(e) and are demarcated by dashed lines. The dark layers correspond to the Er 316LSi, while the light contrast layers correspond to Er NiCrMo-13 material. Distinct solidification phenomenon is observed. The bottom layers of both the materials exhibit equiaxed dendritic structure. In the

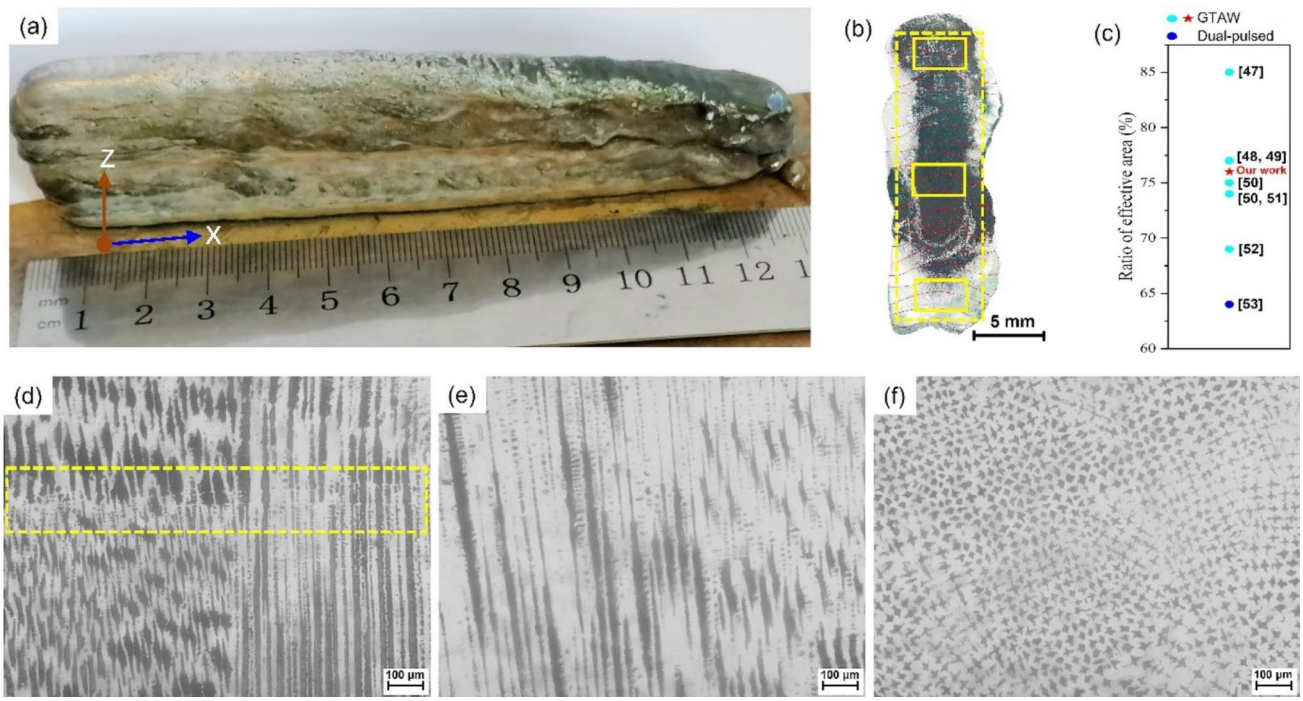

Fig. 9 (**a**) Single wire (Er NiCrMo-13) multi-layer deposition, (**b**) cross section, (**c**) deposition efficiency analysis of single wire deposition, (**d**, **e**, **f**) bottom, middle, and top region microstructure

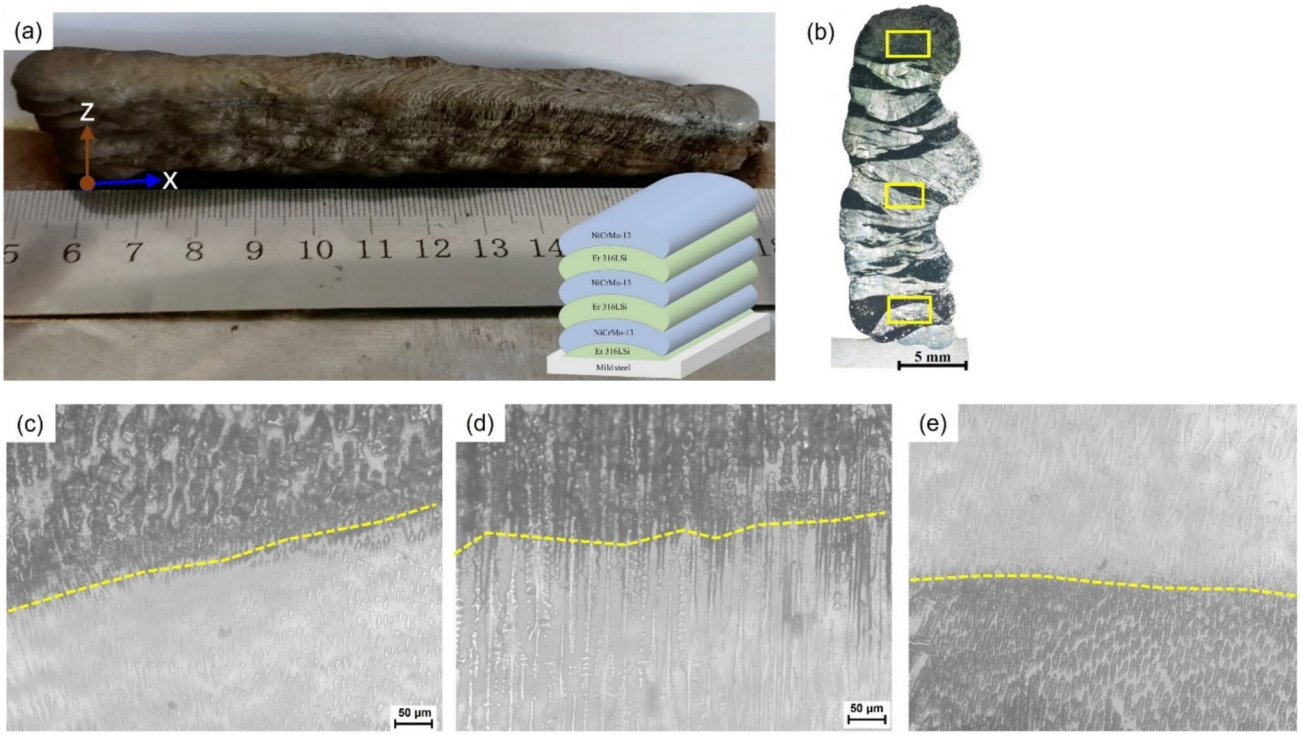

Fig. 10 (**a**) Twin wire (Er NiCrMo-13 + Er 316L Si) multi-layer deposition, (**b**) cross section, (**c**, **d**, **e**) top, middle, and bottom region microstructure

middle regions, columnar dendritic structures are observed. While at the top region equiaxed structure is observed; however, for Er 316LSi, columnar dendritic structure is seen. This difference is typically due to disparate thermophysical properties corresponding to evolving temperature gradients and cooling rates [65, 66]. However, the motion control repeatability and coordinated operation of interconnected systems is successfully demonstrated. As the deposition further progressed sequentially in the build direction, the bead began to slope downward and eventually wall collapse was observed. This phenomenon can be attributed to inherent WAAM process characteristics as outlined below.

At the onset of deposition (arc ignition) and at its completion (arc extinguishing), the bead geometry was not uniform. Humping at start and slope at the end were observed, due to backward fluid flow causing the molten pool swelling at the trailing edge along the deposition direction. This effect is further aggravated with increasing number of layers primarily due to heat build-up from previously deposited layers, which increases thermal inertia proportionally. And the heat dissipation through the substrate progressively decreases and more pronouncedly at the terminal region of the wall, where absence of an adequate heat sink causes thermal accumulation, leading to collapse [67, 68]. To mitigate slopping and collapse issues, two approaches are recommended: optimizing interlayer parameters or using an in situ forced convective cooling system to manage thermal build up [69, 70]. However, implementation of these improvements requires a detailed analysis and setup which is beyond the scope of the present study. Height errors during the initial stages of multi-layer builds caused a staircase effect but were effectively minimized through trajectory control. This adaption ensured smoother transitions and minimized abrupt changes [71, 72].

4.2 Multi-bead deposition

In this section a single-layer multi-bead deposition in unidirectional path, with bead deposition in the X axis and subsequent overlapping along the Y axis, is depicted in Fig. 11. Defect-free depositions were achieved using tool steel wire (M SG 5-GZ-350 as per DIN 8555) with a diameter of 1.2 mm. Multiple bead-on-plate trials were conducted to optimize parameters, with overlapping distance of 60% (a critical parameter which was obtained with reference to literature [73]). Multi-layer deposition is avoided which would necessitate the adaption of heat management strategies as discussed in the previous section. Downward sloping and collapse issues were mitigated by effective heat conduction through the substrate, highlighting the repeatability and reliability of the interconnected systems. A deposition efficiency of 72% was achieved with the layers exhibiting

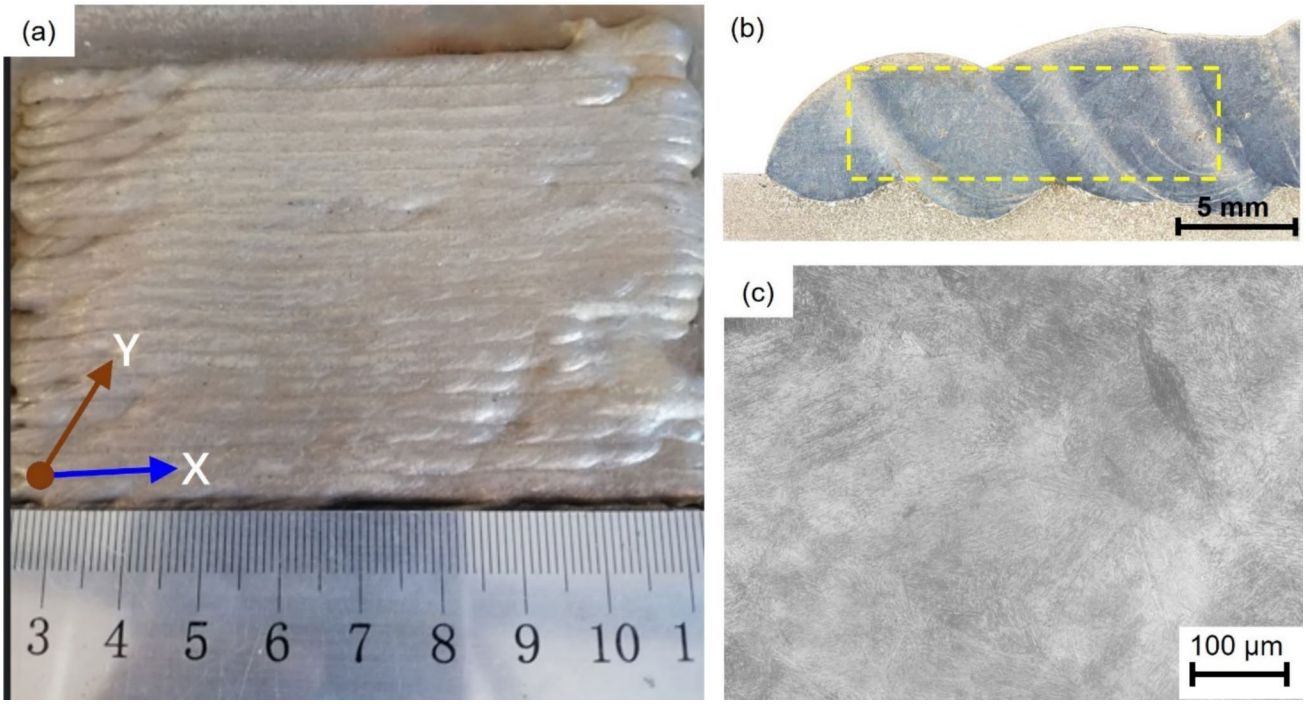

Fig. 11 (**a**) Multi-bead deposition (DIN8555), (**b**) cross section, (**c**) microstructure

good adhesion to the mild steel substrate, demonstrating stability of process parameters employed. The cross section of deposition as shown in Fig. 11 (b) shows no significant irregularities that would compromise the structural integrity of the component. Needle-like structure could be observed in Fig. 11 (c). Due to the direct contact of the deposition layers with the substrate, rapid heat dissipation facilitates the martensite phase transformation [74, 75].

It is evident that from the multi-layer deposition, shown in Fig. 9, Fig. 10, and multi-bead deposition, depicted in Fig. 11, a deposition efficiency exceeding 70% can be achieved. This demonstrates the machine capability to handle diverse geometry paths including thin wall and thick wall structures. Additionally, it can support multiple processes such as WAAM, surface coating, and welding (in autogenous and with filler wire modes) with the addition of clamps to the substrate fixture. The self-developed nature of the machine allows for customization and scalability, enabling it to be tailored specific process.

While the current work does not showcase complex or intricate designs, which require significant advancements in process analysis and development, it establishes a strong foundation for future efforts. In this study, we have effectively demonstrated that the WAAM machine is capable of achieving high deposition efficiencies (exceeding 70%) while maintaining defect-free geometries. These results are directly attributed to key design decisions made during the system's development. The synchronized operation of the twin wire feeder and welder, controlled by the 32-bit control boards, ensured seamless material transitions with precision. Additionally, adaptive trajectory control successfully mitigated staircase effects, resulting in smoother layer transitions and enhanced structural integrity. The self-developed nature of this machine offers scalability and customization capabilities leveraging open-source solutions, supporting multiple processes such as WAAM, surface coating, and welding. These features make this design highly adaptable to continuously evolving requirements of WAAM technology, mitigating the need for costly proprietary upgrades, reducing developmental time. The machine's flexibility, reliability, and adaptability positions it as a robust platform for future advancements in complex shape fabrication and multi-material deposition.

5 Conclusions

Machine building for WAAM requires a multi-faceted approach that integrates diverse systems to execute coordinated set of operations. Commercial and off-the-shelf WAAM setup often limits adaptability, making it challenging to implement in situ auxiliary processes critical for advancing industrial adoption. This study provides a comprehensive framework for designing and building an open-source WAAM machine, ensuring scalability for future

technological needs while promoting cost-effective and customizable solutions.

Key contributions of this work include:

- Motion control system: A detailed analysis of various hardware components and software used, covering selection criteria and limitations, offering users a holistic approach to design and build customized setup modular for multiple processes.
- Electromagnetic compatibility: Effective measures to ensure compatibility were discussed and implemented to ensure operational stability of interconnected systems. These measures are critical for mitigating disruptions commonly encountered in arc-based manufacturing process.
- Welder and wire feeder configuration: The welder and custom-built twin wire feeder system configuration is elaborated and their harmonious interoperability with the motion control system is validated through successful multi-layer and multi-bead depositions.
- Material selection: Optimized material selection such as aluminum profiles and mild steel for structural components ensured durability and cost-effectiveness. The machine design emphasizes vibration resistance, critical for maintaining structural integrity and performance.

This study highlights how 3D printing, as a cornerstone of Industry 4.0, offers smart manufacturing solutions by enabling design freedom and customization. By overcoming scalability constraints inherent in commercial setups, this self-built approach empowers the WAAM community to develop tailored solutions, while fostering innovation.

Additionally, the flexibility of this machine opens avenues for future applications such as hybrid WAAM systems combining additive and subtractive processes or integrating advanced monitoring systems for autonomous operation. By leveraging open-source frameworks, this work significantly impacts the WAAM community by reducing costs, expanding accessibility, and advancing metal additive manufacturing in alignment with Industry 4.0 principles.

Supplementary Information The online version contains supplementary material available at https://doi.org/10.1007/s00170-025-15754-x.

Author contribution All authors contributed to the study conception, design, and development. Conception, development, stabilization, and programming were performed by Nithin Joseph Reddy Sagili Arthur. Design were performed by Liu Lei and supported in development and stabilization. Resources, supervision, and validation were performed by Prof. João Pedro Oliveira. The first draft of the manuscript was written by Nithin Joseph Reddy Sagili Arthur and all authors commented on previous versions of the manuscript. All authors read and approved the final manuscript.

Funding Open access funding provided by FCT|FCCN (b-on). Nithin Joseph Reddy Sagili Arthur received funding from Fundação para a Ciência e a Tecnologia (FCT) for its financial support via the PhD grant 2022.10356.BD. Lei Liu received the financial support from the China Scholarship Council Grant No. 202208420052. The authors also received funding by national funds from FCT—Fundação para a Ciência e a Tecnologia, I.P., in the scope of the project's LA/P/0037/2020, UIDP/50025/2020, and UIDB/50025/2020 of the Associate Laboratory Institute of Nanostructures, Nanomodelling and Nanofabrication – i3N.

Declarations

Competing interests The authors declare no competing interests.

References

1. ShojaeiBarjuei E, Courteille E, Rangeard D et al (2022) Real-time vision-based control of industrial manipulators for layer-width setting in concrete 3D printing applications. Adv Ind Manuf Eng 5:100094. https://doi.org/10.1016/j.aime.2022.100094
2. Khosravani MR, Nasiri S, Reinicke T (2022) Intelligent knowledge-based system to improve injection molding process. J Ind Inf Integr 25:100275. https://doi.org/10.1016/j.jii.2021.100275
3. Stavropoulos P, Pastras G, Tzimanis K, Bourlesas N (2024) Addressing the challenge of process stability control in wire DED-LB/M process. CIRP Ann 73:129–132. https://doi.org/10.1016/j.cirp.2024.04.021
4. Shah A, Aliyev R, Zeidler H, Krinke S (2023) A review of the recent developments and challenges in wire arc additive manufacturing (WAAM) process. J Manuf Mater Process 7:97. https://doi.org/10.3390/jmmp7030097
5. Yang J, Kyvelou P, Wadee MA, Gardner L (2024) Simulation and prediction of residual stresses in WAAM-strengthened I-sections. Structures 69:107248. https://doi.org/10.1016/j.istruc.2024.107248
6. Li Y, Su C, Zhu J (2022) Comprehensive review of wire arc additive manufacturing: hardware system, physical process, monitoring, property characterization, application and future prospects. Results Eng 13:100330. https://doi.org/10.1016/j.rineng.2021.100330
7. Saleh B, Fathi R, Tian Y et al (2023) Fundamentals and advances of wire arc additive manufacturing: materials, process parameters, potential applications, and future trends. Arch Civil Mech Eng 23:96. https://doi.org/10.1007/s43452-023-00633-7
8. Davoudinejad A, Khosravani MR, Pedersen DB, Tosello G (2020) Influence of thermal ageing on the fracture and lifetime of additively manufactured mold inserts. Eng Fail Anal 115:104694. https://doi.org/10.1016/j.engfailanal.2020.104694
9. Karouanas I, Foteinopoulos P, Bikas H, Stavropoulos P (2024) A practical simulation approach for the support of wire arc DED additive manufacturing systems design. In: Procedia Computer

Science. Elsevier B.V., pp 3161–3172. https://doi.org/10.1016/j.procs.2024.02.132
10. Huang J, Li Z, Yu S et al (2022) Real-time observation and numerical simulation of the molten pool flow and mass transfer behavior during wire arc additive manufacturing. Weld World 66:481–494. https://doi.org/10.1007/s40194-021-01214-z
11. Xia C, Pan Z, Polden J et al (2020) A review on wire arc additive manufacturing: monitoring, control and a framework of automated system. J Manuf Syst 57:31–45. https://doi.org/10.1016/j.jmsy.2020.08.008
12. Abe T, Kaneko J, Sasahara H (2020) Thermal sensing and heat input control for thin-walled structure building based on numerical simulation for wire and arc additive manufacturing. Addit Manuf 35:101357. https://doi.org/10.1016/j.addma.2020.101357
13. Kiran A, Kumar H, Sivanandam S et al (2025) Explainable AI in thermal modelling enhancing precision in thermal gradient monitoring for additive manufacturing using LSTM networks. Therm Sci Eng Prog 60:103465. https://doi.org/10.1016/j.tsep.2025.103465
14. Xiong J, Liu G, Zhang G (2023) Influence of interlayer temperature on microstructure and mechanical properties of TiAl alloys in wire and arc additive manufacturing. J Manuf Process 94:278–288. https://doi.org/10.1016/j.jmapro.2023.03.062
15. Théodore J, Couturier L, Girault B et al (2023) Relationship between microstructure, and residual strain and stress in stainless steels in-situ alloyed by double-wire arc additive manufacturing (D-WAAM) process. Materialia (Oxf) 30:101850. https://doi.org/10.1016/j.mtla.2023.101850
16. Anzalone GC, Zhang C, Wijnen B et al (2013) A low-cost open-source metal 3-D printer. IEEE Access 1:803–810
17. Yilmaz O, Almusawi ARJ (2015) Design, construction, and controlling of a shaped metal deposition machine using arc metal-wire system. Conference: 8th international conference and exhibition on design and production of machines and dies/molds. Volume: 8. Izmir, Turkey
18. Khaudair HJ, Ugla AA, Almusawi ARJ (2021) Design, integrating and controlling of MIG-based shaped metal deposition system with externally cold wire feed in additive layered manufacturing technology. Arab J Sci Eng 46:2677–2690. https://doi.org/10.1007/s13369-020-05100-6
19. Prado-Cerqueira JL, Diéguez JL, Camacho AM (2017) Preliminary development of a wire and arc additive manufacturing system (WAAM). Procedia Manuf 13:895–902. https://doi.org/10.1016/j.promfg.2017.09.154
20. Lu X, Zhou YF, Xing XL et al (2017) Open-source wire and arc additive manufacturing system: formability, microstructures, and mechanical properties. Int J Adv Manuf Technol 93:2145–2154. https://doi.org/10.1007/s00170-017-0636-z
21. Rosli NA, Alkahari MR, Ramli FR et al (2018) Design and development of a low-cost 3d metal printer. J Mech Eng Res Dev 41:47–54. https://doi.org/10.26480/jmerd.03.2018.47.54
22. Khan AU, Madhukar YK (2020) An economic design and development of the wire arc additive manufacturing setup. In: Procedia CIRP. Elsevier B.V., pp 182–187. https://doi.org/10.1016/j.procir.2020.02.166
23. Navarro M, Matar A, Diltemiz SF, Eshraghi M (2022) Development of a low-cost wire arc additive manufacturing system. J Manuf Mater Process 6:3. https://doi.org/10.3390/jmmp6010003
24. Bandari Y, Ding J, Bandari YK et al (2015) Additive manufacture of large structures: robotic or CNC systems. In Proceeding of the 26th international solid freeform fabrication symposium, Austin, Texas
25. Dyvik SH, Manum B, Haddal J et al (2019) Structural aluminium in architecture-the history and future of aluminium as a structural material. The international conference on structures and architecture, Lisbon, Portugal
26. Tabe H Crack resistance of hardened steels against thermal shock. In Proceedings of the 6th international tooling conference, Japan
27. Kramer T, Proctor F, Messina E (2000) The NIST RS274NGC interpreter - version 3, NIST interagency/internal report (NISTIR), national institute of standards and technology, Gaithersburg, MD, [online], https://tsapps.nist.gov/publication/get_pdf.cfm?pub_id=823374. Accessed 26 Oct 2024
28. Formentini G, Boix Rodríguez N, Favi C (2022) Design for manufacturing and assembly methods in the product development process of mechanical products: a systematic literature review. Int J Adv Manuf Technol 120:4307–4334. https://doi.org/10.1007/s00170-022-08837-6
29. Selvaraj P, Radhakrishnan P, Adithan M (2009) An integrated approach to design for manufacturing and assembly based on reduction of product development time and cost. Int J Adv Manuf Technol 42:13–29. https://doi.org/10.1007/s00170-008-1580-8
30. Oriental Motor Technology – Motor Sizing Calculations. https://www.orientalmotor.com/technology/motor-sizing-calculations.html [Accessed 26 October 2024]
31. NEMA ICS 16 (2001) Motion/position control motors, controls and feedback devices. https://www.nema.org/standards/view/motion-position-control-motors-controls-and-feedback-devices. Accessed 26 Oct 2024
32. LDO Motors – NEMA 23 Stepper Motor Specifications. https://ldomotors.com/products/show/57mm-hybrid-stepper-series [Accessed 01 April 2025]
33. Norton RL (1999) Design for machinery : an introduction to the synthesis and analysis of mechanisms and machines, 2nd edn. McGraw-Hill, New York
34. OPENBUILDS – linear screw specifications. https://us.openbuilds.com/8mm-metric-lead-screw/ [Accessed 01 April 2025]
35. Budynas RG, Nisbett JK (2015) Shigley's mechanical engineering design, 10th edn. McGraw-Hill Education, New York
36. Duet3D. https://www.duet3d.com [Accessed 26 October 2024]
37. BigTreeTech. https://bigtree-tech.com [Accessed 26 October 2024]
38. Lerdge. https://shop.lerdge.com [Accessed 26 October 2024]
39. Smoothieboard. https://www.kickstarter.com/projects/arthurwolf/smoothieboard-v2 [Accessed 26 October 2024]
40. Panucatt. https://www.panucatt.com [Accessed 26 October 2024]
41. Aus3D. https://aus3d.com.au [Accessed 26 October 2024]
42. Max3D Shop. https://max3dshop.org [Accessed 26 October 2024]
43. BeagleBoard. https://www.beagleboard.org [Accessed 26 October 2024]
44. Marlin firmware and kinematics. https://marlinfw.org/docs/configuration/configuration.html#kinematics [Accessed 26 October 2024]
45. Klipper firmware and kinematics. https://www.klipper3d.org/Kinematics.html [Accessed 26 October 2024]
46. RepRap firmware and kinematics. https://docs.duet3d.com/User_manual/RepRapFirmware/RepRapFirmware_overview [Accessed 26 October 2024]
47. Repeiter firmware and kinematics. https://docfirmwarev2.repetier.com/config/printer_type [Accessed 26 October 2024]
48. Replicape firmware and kinematics . https://replicape.github.io/replicape/configuration.html [Accessed 26 October 2024]
49. ISO (13850:2015) Safety of machinery-Emergency stop function-Principles for design. https://www.iso.org/obp/ui/en/#iso:std:59970:en. Accessed 26 Oct 2024
50. Gokhale NP, Gadakh DA, Kala P (2021) Effect of arc polarity on the quality of deposition in GTAW welding-based additive manufacturing process: a preliminary study. J Adv Manuf Syst 21:337–349. https://doi.org/10.1142/S0219686722500093
51. Choudhury SS, Marya SK, Amirthalingam M (2021) Improving arc stability during wire arc additive manufacturing of thin-walled

titanium components. J Manuf Process 66:53–69. https://doi.org/10.1016/j.jmapro.2021.03.033
52. American National Standard Dictionary of Electromagnetic Compatibility (EMC) including electromagnetic environmental effects (E3) - redline," in ANSI C63.14-2014 (Revision of ANSI C63.14-2009) - Redline. pp.1–152
53. Hoolihan DD (2021) NEW STANDARD PUBLISHED: C63.24 - American national standard: recommended practice for in Situ RF immunity evaluation of electronic devices and systems. In IEEE electromagnetic compatibility magazine. 10(3):97–97. https://doi.org/10.1109/MEMC.2021.9614263
54. Martina F, Mehnen J, Williams SW et al (2012) Investigation of the benefits of plasma deposition for the additive layer manufacture of Ti-6Al-4V. J Mater Process Technol 212:1377–1386. https://doi.org/10.1016/j.jmatprotec.2012.02.002
55. Alberti EA, Bueno BMP, D'Oliveira ASCM (2016) Additive manufacturing using plasma transferred arc. Int J Adv Manuf Technol 83:1861–1871. https://doi.org/10.1007/s00170-015-7697-7
56. Chen Y, Yang C, Fan C, Wang M (2022) Microstructure evolution and mechanical properties of a nickel-based superalloy repaired using wire and arc additive manufacturing. Mater Charact 193:112315. https://doi.org/10.1016/j.matchar.2022.112315
57. Tian Y, Chen X, Cai Y et al (2022) Microstructure and properties of a Ni–Ti–Cr–Mo–Nb alloy fabricated in situ by dual-wire arc additive manufacturing. Mater Sci Eng: A 853:143740. https://doi.org/10.1016/j.msea.2022.143740
58. Zhang M, Wang Y, Yang Z et al (2022) Microstructure and mechanical properties of twin wire and arc additive manufactured Ni3Al-based alloy. J Mater Process Technol 303:117529. https://doi.org/10.1016/j.jmatprotec.2022.117529
59. Sujan GK, Li H, Pan Z, et al (2022) Application of wire arc additive manufacturing for Inconel 718 superalloy. pp 367–410. https://doi.org/10.1007/978-3-030-91873-6_15
60. Mukhrish YE, Asad M, Khan MAA, Djavanroodi F (2023) Experimental investigations on wire arc additive manufacturing process using an Inconel 625 alloy wire. Mech Adv Mater Struct. https://doi.org/10.1080/15376494.2023.2256336
61. Asala G, Khan AK, Andersson J, Ojo OA (2017) Microstructural analyses of ATI 718Plus® produced by wire-ARC additive manufacturing process. Metall Mater Trans A Phys Metall Mater Sci 48:4211–4228. https://doi.org/10.1007/s11661-017-4162-2
62. Zhang G, Zhang C, Zhu M, Shi Y (2024) Effect of high pulse frequency on microstructure and mechanical properties of Inconel 718 alloy prepared by wire filling stepped-dual pulsed GTA-AM. J Manuf Process 124:1037–1052. https://doi.org/10.1016/j.jmapro.2024.06.072
63. Yangfan W, Xizhang C, Chuanchu S (2019) Microstructure and mechanical properties of Inconel 625 fabricated by wire-arc additive manufacturing. Surf Coat Technol 374:116–123. https://doi.org/10.1016/j.surfcoat.2019.05.079
64. Zhang X, Zhai G, Jiang C et al (2024) Hydrogen-induced cracking behaviors of Ni–Cr–Mo-based superalloy fabricated by wire arc additive manufacturing under different solution temperature. Int J Hydrogen Energy 91:901–911. https://doi.org/10.1016/j.ijhydene.2024.10.200
65. Mukherjee T, Wei HL, De A, DebRoy T (2018) Heat and fluid flow in additive manufacturing – part II: powder bed fusion of stainless steel, and titanium, nickel and aluminum base alloys. Comput Mater Sci 150:369–380. https://doi.org/10.1016/j.commatsci.2018.04.027
66. Rodrigues TA, Cipriano Farias FW, Zhang K et al (2022) Wire and arc additive manufacturing of 316L stainless steel/Inconel 625 functionally graded material: development and characterization. J Market Res 21:237–251. https://doi.org/10.1016/j.jmrt.2022.08.169
67. Xiong J, Yin Z, Zhang W (2016) Forming appearance control of arc striking and extinguishing area in multi-layer single-pass GMAW-based additive manufacturing. Int J Adv Manuf Technol 87:579–586. https://doi.org/10.1007/s00170-016-8543-2
68. Hu Z, Qin X, Shao T, Liu H (2018) Understanding and overcoming of abnormity at start and end of the weld bead in additive manufacturing with GMAW. Int J Adv Manuf Technol 95:2357–2368. https://doi.org/10.1007/s00170-017-1392-9
69. Dinovitzer M, Chen X, Laliberte J et al (2019) Effect of wire and arc additive manufacturing (WAAM) process parameters on bead geometry and microstructure. Addit Manuf 26:138–146. https://doi.org/10.1016/j.addma.2018.12.013
70. Wu B, Pan Z, Ding D et al (2018) The effects of forced interpass cooling on the material properties of wire arc additively manufactured Ti6Al4V alloy. J Mater Process Technol 258:97–105. https://doi.org/10.1016/j.jmatprotec.2018.03.024
71. Singh P, Dutta D Multi-direction layered deposition - an overview of process planning methodologies. In Proceeding of the 2003 Solid Freeform Fabrication Symposium. https://doi.org/10.26153/tsw/5563
72. Li Y, Huang X, Horváth I, Zhang G (2018) GMAW-based additive manufacturing of inclined multi-layer multi-bead parts with flat-position deposition. J Mater Process Technol 262:359–371. https://doi.org/10.1016/j.jmatprotec.2018.07.010
73. Han Q, Li X, Dong M, Zhang G (2021) Enhanced curve-fitting model of the bead section profile and the corresponding overlapping model for twin-electrode gas tungsten arc-based additive manufacturing. Int J Adv Manuf Technol 116(3):1151–1167. https://doi.org/10.1007/s00170-021-07501-9
74. Pixner F, Buzolin R, Warchomicka F et al (2023) Influence of process and heat input on the microstructure and mechanical properties in wire arc additive manufacturing of hot work tool steels. Mater Sci Eng: A 888:145799. https://doi.org/10.1016/j.msea.2023.145799
75. Pixner F, Buzolin R, Zelić A et al (2022) Tailoring the alloy composition for wire arc additive manufacturing utilizing metal-cored wires in the cold metal transfer process. Mater Des 215:110453. https://doi.org/10.1016/j.matdes.2022.110453